Dynamic instability of the intracellular pressure drives bleb-based motility

Benoît Maugis[1,2], Jan Brugués[3], Pierre Nassoy[1,2], Nancy Guillen[4,5], Pierre Sens[3] and François Amblard[1,2,*]

[1]Institut Curie, Centre de Recherche, Paris, 75248, France
[2]CNRS, UMR168, Paris, 75248, France
[3]Laboratoire Gulliver, CNRS-ESPCI, UMR 7083, Paris, 75231, France
[4]Institut Pasteur, Unité de Biologie Cellulaire du Parasitisme, Paris, 75015, France
[5]INSERM U786, Paris, 75015, France
*Author for correspondence (francois.amblard@curie.fr)

Accepted 27 July 2010
Journal of Cell Science 123, 3884-3892

doi:10.1242/jcs.065672

Summary

We have demonstrated that the two- and three-dimensional motility of the human pathogenic parasite *Entamoeba histolytica* (*Eh*) depends on sustained instability of the intracellular hydrostatic pressure. This instability drives the cyclic generation and healing of membrane blebs, with typical protrusion velocities of 10–20 μm/second over a few hundred milliseconds and healing times of 10 seconds. The use of a novel micro-electroporation method to control the intracellular pressure enabled us to develop a qualitative model with three parameters: the rate of the myosin-driven internal pressure increase; the critical disjunction stress of membrane–cytoskeleton bonds; and the turnover time of the F-actin cortex. Although blebs occur randomly in space and irregularly time, they can be forced to occur with a defined periodicity in confined geometries, thus confirming our model. Given the highly efficient bleb-based motility of *Eh* in vitro and in vivo, *Eh* cells represent a unique model for studying the physical and biological aspects of amoeboid versus mesenchymal motility in two- and three-dimensional environments.

Key words: Blebs, Cytoskeleton, Motility

Introduction

On the basis of extensive investigations in different cell types and in various contexts, two distinct modes of cell motility (mesenchymal and amoeboid motility) have been proposed (Friedl and Wolf, 2003; Sahai, 2007). These modes differ in many respects: cell morphology, the organization and dynamics of cell–substrate adhesion, the localization and activity of the actomyosin contractile machinery, and the distribution of the forces exerted on two-dimensional (2D) and three-dimensional (3D) substrates (Bray, 2001; Mierke et al., 2008). It has also been reported that some cells can undergo a transition between these modes (Friedl and Wolf, 2003; Friedl, 2004), and that the motility mode strongly influences migration efficiency (Carragher et al., 2006). It is therefore likely that cells optimize their motility by selecting distinct strategies, probably as a function of the state of their molecular 'machinery' and of their environment. This optimization could be relevant for metastatic invasion, leukocyte migration in lymph nodes or target tissues, and cell movements during embryonic development, where cells successively encounter different 3D contexts (Hugues et al., 2004; Raz and Reichman-Fried, 2006). For instance, during immune surveillance and the inflammatory response, leukocytes move through environments such as blood, mucus, epithelium and the lymphatic circulatory system (Hugues et al., 2004). We studied *Entamoeba histolytica* (*Eh*) cells, the causative agent of amoebiasis (dysentery) (Stanley, 2003). This pathogen passes through various environments (intestinal tissue layers, the portal vein and the liver microcirculation) as it invades and ultimately destroys the host intestine and produces liver abscesses (Stanley, 2001). Given this context, the objective of the present work was to elucidate the physical basis of *Eh* cell motility and elaborate a model of amoeboid behavior, with special focus on the role of the internal hydrostatic pressure.

In previous work using in vivo two-photon imaging, we observed that *Eh* migration in the liver during the infectious process is accompanied by very intense, cyclic production of spherical protrusions of the plasma membrane (Coudrier et al., 2005). In vitro, these protrusions can either retract or become stable and thus sustain the exploration of the local environment by the cell over several hours (Coudrier et al., 2005). In the absence of externally guided cell motility, there is no correlation between the directions of the protrusions, and efficient, random exploration of the substrate is observed. However, appropriate chemotactic gradients do orient and stabilize protrusions in particular directions (Blazquez et al., 2006; Zaki et al., 2006). It is known that myosin II is essential for *Eh* motility, both in vitro (Arhets et al., 1998) and in vivo (Coudrier et al., 2005). In the present work, we demonstrated that the *Eh* cell protrusions are blebs (Keller et al., 2002; Fackler and Grosse, 2008; Charras and Paluch, 2008). By studying the mechanism underlying their production, we further showed that the blebs directly actuate cell motility in a physiological context. Our observations suggest that *Eh* cells could serve as a valuable prototype for studying amoeboid motility in general.

Results

Spherical protrusions produced in 3D, 2D and liquid environments

Infection by *Eh* requires efficient motility through environments that vary in terms of their geometrical, mechanical and biochemical properties. In an initial report (Coudrier et al., 2005), we observed a strong correlation between the efficiency of the infectious process (as measured experimentally in animal models), in vivo cell motility and the active generation of cell protrusions. Here, we show that these protrusions are spherical and thus very distinct from the

lamellipodia and filopodia involved in mesenchymal migration. Protrusion generation is similarly active in both 2D and 3D, as shown in the 3D liver parenchyma (supplementary material Movie 1) and on bare glass (supplementary material Movie 2). This suggests that the microenvironment in contact with the cell has a limited effect on protrusive activity. To further assess the role of cell–substrate contacts, amoebae were loaded at the interface between two fluids of differing density (a Percoll solution and culture medium). In this fluid environment, cells continue to actively produce round protrusions (supplementary material Movie 3). Similarly, when cells simply sediment through culture medium, active protrusions are still observed and persist once contact with the substrate is made (supplementary material Movie 4). These results clearly indicate that the protrusive activity is intrinsic to amoeba cells and is not induced by cell–substrate adhesion.

Relationship between motility and asymmetric and dynamic contacts

Because *Eh* cells do not have specialized organelles for moving in liquids (e.g. flagella or cilia), they can only achieve net motion relative to their environment by interacting with a solid substrate. Although no net motion is observed in floating or sedimenting cells (supplementary material Movies 3 and 4), the latter start to move as soon as they contact with the substrate, which suggests an ability to transfer momentum.

To further investigate cell–substrate contact and its role in protrusive activity, we combined conventional phase-contrast imaging with the observation of adhesion patterns using reflection interference contrast microscopy (RICM) (Fig. 1; supplementary material Movie 5 and Fig. S3). Strikingly, the shape of *Eh* cells is quite distinct from their contacting surface; this is in contrast to fibroblasts and most adherent cells, for which adhesion strongly dictates the cell profile. Despite extended regions of tight contact (revealed by continuous zones of dark RICM signal), the production of protrusions leads to discontinuous contact zones away from the tight contact area (Fig. 1B). This observation indicates that protrusions are produced as elevated structures that can contact the substrate at a remote site. This is in agreement with observations of 3D protrusions in a liquid environment (supplementary material Movie 3) and with previous electron microscopy pictures (Gonzalez-Robles and Martinez-Palomo, 1983) showing that protrusions are triggered all around the cell surface (which has a typical size of 20 µm in all three dimensions).

The initial, discontinuous contacts then either nucleate and grow into larger surfaces (which eventually bridge with the main zone (supplementary material Fig. S3) or disappear if the protrusions retract. Hence, protrusion dynamics is coupled to dynamic spreading of adhesive contacts. The cell boundary seen in phase-contrast microscopy always extends beyond the dark RICM zone, indicating an ‘overhang’ type of geometry (sketched in Fig. 1D). Interestingly, this overhang is much greater in protruding regions than in retracting regions. This clear asymmetry can be interpreted as a contact angle difference, which is probably due to the plasma membrane and the associated cortex being peeled away in retracting zones.

For further investigation of the protrusion mechanism of *Eh* cells, it is important to note that cell–glass adhesion forces (which could in principle lead to an extensive contact area and a rather flat morphology) are dominated by the contraction-induced and elastic forces inside the cortex. These forces probably drive cell deformation in 2D and in 3D, as mentioned above. Nevertheless, the adhesion forces are strong enough to produce effective contacts and the momentum transfer required for the observed motility. In principle, the adhesive interactions are not specific on the molecular level, despite the surface expression of specific adhesion receptors (Coudrier et al., 2005). Indeed, similar motile behaviors have been observed on substrates with greater or lower hydrophobicity than bare glass (supplementary material Figs S1 and S2). These observations indicate that excessive adhesion could inhibit the production of *Eh* cell protrusions, as reported elsewhere (Friedl et al., 2001).

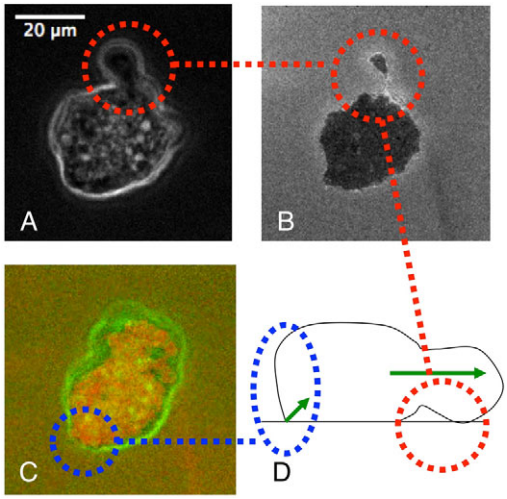

Fig. 1. Comparative geometry and dynamics of protrusions and adhesion. An *Eh* cell was simultaneously imaged in (**A**) phase-contrast microscopy and (**B**) reflection interference contrast microscopy (RICM). In RICM, dark regions correspond to areas of cell–substrate contact closer than 100 nm. The expanding protrusion makes discrete contact with the substrate and expands beyond the contact region. A few seconds later, overlaid phase-contrast (green) and RICM (red) images (**C**) show the lateral extension of non-contacting regions of the cell. A larger overhang is observed (**D**) in the protruding region (red) than in the contracting cortex (blue), probably due to a ‘peeling’ effect. Arrows indicate the directions of expansion and contraction. This behavior was reproducibly observed with seven cells.

Plasma membrane abruptly detaches from the cytoskeleton

We next focused on the physical mechanism underlying protrusive activity by *Eh* cells moving on a glass surface. The results presented in the preceding section indicated that adhesion does not directly interfere with the intracellular processes that lead to protrusion production, which can be considered as operating independently of contact with the substrate. Phase-contrast video microscopy observations revealed deformations of the cell boundary on two distinct time scales: slow (10–30 seconds) overall changes (supplementary material Movie 6) and fast (0.1–5 seconds) local changes (supplementary material Movie 7). The slow, overall deformations exhibit a constant phase-contrast pattern, suggesting a stationary cell cortex structure. By contrast, fast deformations are protrusions that correspond locally to major changes in the phase-contrast signal; this indicates that the cortical structure is strongly modified. Interestingly, myosin inhibition produces conditions under which fast deformations are blocked and slow deformations

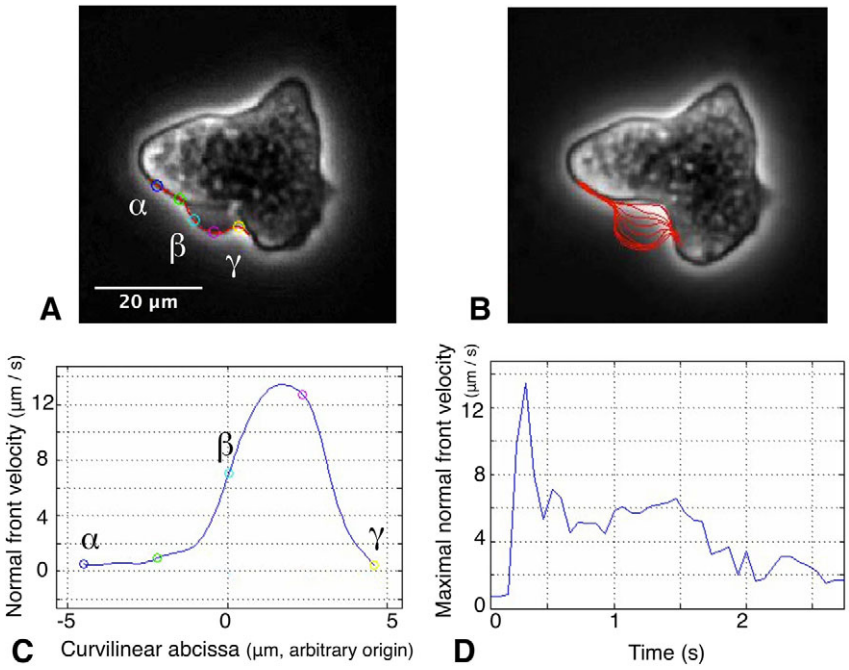

Fig. 2. Geometry and kinetics of contour deformations. Edges were (**A**) detected on individual images by autocorrelation analysis (see Materials and Methods) and (**B**) monitored over time at a 15 Hz frame rate. Each contour was analyzed in terms of the local front speed and curvature. (**C**) Speed is shown as a function of the curvilinear abscissa. Three points on the contour (α, β, γ) were used to visualize the match between A and C. (**D**) Peak speed is shown as function of time. The peak speed curve shows a burst that reaches 13 μm/second. Similar results were found with n=10 cells, with peak front speeds of up to 20 μm/second.

persist (supplementary material Fig. S4C,E); motility is much reduced, indicating that fast protrusions are essential and that slow deformations practically do not contribute to mobility. Time-lapse video analysis using a 15 Hz frame rate (Fig. 2) shows that protrusions expand at remarkably high speeds. Indeed, velocities as high as 10–20 μm/second are typically observed during the first few hundred milliseconds of expansion.

A straightforward scaling argument (see Materials and Methods) leads to a simple equation between the pressure difference δP, the fluid velocity v, the cytosol viscosity η, the mesh size ξ and the thickness h of the cortex: $\delta P \simeq \eta v h \xi^{-2}$. An order of magnitude estimation (with $\eta=10^{-3}$ Pa seconds, v=10 μm/seconds, ξ=30–100 nm and h=1 μm) indicates that a pressure difference of around 1–10 Pa is enough to account for the observed velocity.

At the onset of protrusion production, the membrane moves away from the initial cell boundary, whereas the contrast associated with the latter does not move. The advancing front can be broad (5–10 μm in width) and shows a uniform curvature and much weaker contrast than the boundary from which it originated (supplementary material Movie 7). This observation suggests that the plasma membrane is no longer underpinned by the cortical cytoskeleton. Meanwhile, the contrast associated with the initial contour remains intact for a few seconds, indicating that the cortex itself also remains intact. Furthermore, the inside of the protrusion initially shows a uniform, structure-free background signal that contrasts strongly with the granularity of rest of the cytosol. However, a few seconds later, the initial cortex starts to gradually disappear and organelles invade the protrusion (supplementary material Movie 8).

This set of observations shows that the plasma membrane abruptly detaches from the underlying cortex on a time scale (typically less than 0.1 second) over which the structure of the actin cortex does not change. This observation agrees with the fact that actin polymerization fronts are typically much slower (around 0.1 μm/second) (Pollard, 1986; Theriot et al., 1992) than the front velocities measured here. Furthermore, the observed velocities are similar to other 'explosive' processes that are not powered by polymerization, such as the *Thyone* acrosomal process (Tilney and Inoue, 1985). Our observations strongly suggest that *Eh* cell protrusions are bona fide blebs, as indicated by their sphericity, the absence of submembrane structure and the hyaline-like appearance of the inner face. Protrusion production via membrane disjunction is analogous to the formation of apoptotic blebs by proteolytic cleavage of cytoskeleton–membrane links (Mills et al., 1998; Mills et al., 1999). Unlike necrotic blebs, *Eh* blebs are highly dynamic in nature; rapid expansion is followed by cytosol invasion and gradual association between the membrane and a new cortex. These events occur in a cyclic fashion.

On the molecular level, the actin cortex (seen in parallel time-lapse videos of phase contrast and F-actin fluorescence; Fig. 3) shows fast disjunction, with no change in the fluorescence of the initial structure. However, 4 seconds later, the fluorescence decays and the rim of the bleb becomes fluorescent (indicating the accumulation of F-actin).

The time courses of F-actin dynamics along the initial cortex and along the bleb rim (Fig. 4A) are shown as a series of kymographs (Fig. 4B,C) and are integrated over time (Fig. 4D,E). These semiquantitative data indicate that the typical times for depolymerization and distal repolymerization are similar (on the order of 5–10 seconds). This is in agreement with the notion that the F-actin cortex turns over constantly, with the balance between depolymerization and polymerization rates at the plasma membrane possibly leading to a steady-state cortex in the absence of disruption (Fig. 4F) and simultaneous collapse/repolymerization in the event of disjunction.

The preceding observations are schematically summarized in Fig. 5A. Blebs drive the net motion of the cells via three schematic transitions occurring on different time-scales. From the initial state (a), the plasma membrane detaches from the cytoskeleton (typically within 0.1 seconds). From the second state (b), the cytoskeleton gradually depolymerizes and repolymerizes under the bleb membrane (c). Within 5–10 seconds, the 'old' cortex has vanished

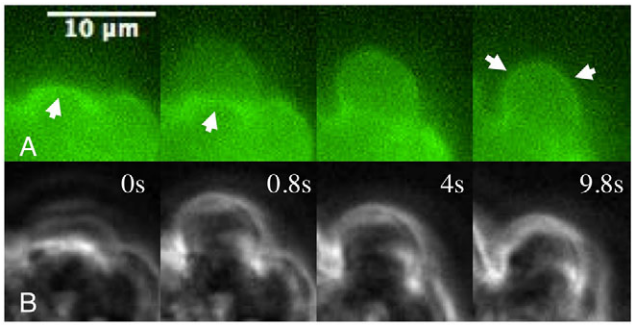

Fig. 3. Localization of F-actin during bleb formation. (**A**) Fluorescent actin cortex images and (**B**) time-lapse phase-contrast images during protrusion generation and stabilization. Actin is revealed by LifeAct–GFP (exposure time 2×60 milliseconds) synchronously interleaved with phase images (exposure time 60 milliseconds). In qualitative terms, the initial cortex gradually disappears within 10 seconds (arrows on the images at 0 and 0.8 seconds), while the new cortex forms at the edge of the stable bleb (arrows on the image at 9.8 seconds). A quantitative analysis of the polymerization/depolymerization kinetics is shown in Fig. 4.

and the new cortex has fully matured (d). In this situation, contraction forces can deform the cell and eventually lead to a new disjunction.

Analysis of forces and proposal of a cyclic model

Most investigations of cell motility have focused on situations in which actin polymerization has a dominant role. In these situations the membrane has an ancillary role, which mainly consists of templating actin polymerization while remaining attached to the cortex. Here, given the disjunction, one must reconsider the forces exerted on the linkers by the membrane and the cytoskeleton (Fig. 5B) and their relationship with contractile activity.

The plasma membrane is subjected (Fig. 5B, blue arrows) to hydrostatic pressure from the outside fluid (π_{ext}) and the internal medium (π_{int}). It is also subjected to forces exerted by individual links, the surface density of which yields an effective pressure (π_{links}). Given the mechanical equilibrium of the links (i.e. as long as they hold firm), this pressure also equals the contractile pressure exerted upon the links by the cortex (π_c). The latter is produced by cortical contractile tension (γ_c) and curvature.

After membrane disjunction (Fig. 5B′), a different set of forces must be considered. The linker pressure (π_{links}) on the membrane and its opposing cytoskeletal counterpart disappear. This change corresponds to effective outward pressure of the same magnitude on the membrane, together with effective inward pressure on the cytoskeleton. We also consider that the outward hydrodynamic flux through the cortex leads to viscous resistance (corresponding to outward pressure on the cortex, π_{hydro}). Membrane disjunction implies the local disruption of a large number of non-covalent bonds (a few square micrometers), characterized at the individual level by finite on/off rates. When stressed, the off rate increases exponentially with the stress (Bell, 1978) and an 'avalanche effect' is expected above a critical pressure π^*_{links}, which will directly depend on the density and binding energy of the bond.

As discussed below, variations in the osmotic pressure on the membrane have been neglected because no water influx is observed during protrusion production and resorption. In principle, two additional forces should be considered. First, the membrane is subjected to surface tension that could (along with curvature) slow down or stop bleb expansion. This was suggested by our observation that blebs often exhibit larger front velocities in concave regions (data not shown). This aspect has been considered in a theoretical publication (Brugues et al., 2010) but cannot be easily taken into account in the experiments presented herein. Second, cell–substrate contact generates surface forces at the membrane and primarily prevents local bleb formation. These forces do not impede blebbing in contact-free zones.

On the basis of the above mechanical analysis, we propose a cyclic model (Fig. 5C) in which cortical contraction builds up the inside pressure difference across the plasma membrane to the point where it exceeds the critical disjunction pressure (π^*_{links}) that the linker distribution can withstand. When the membrane detaches

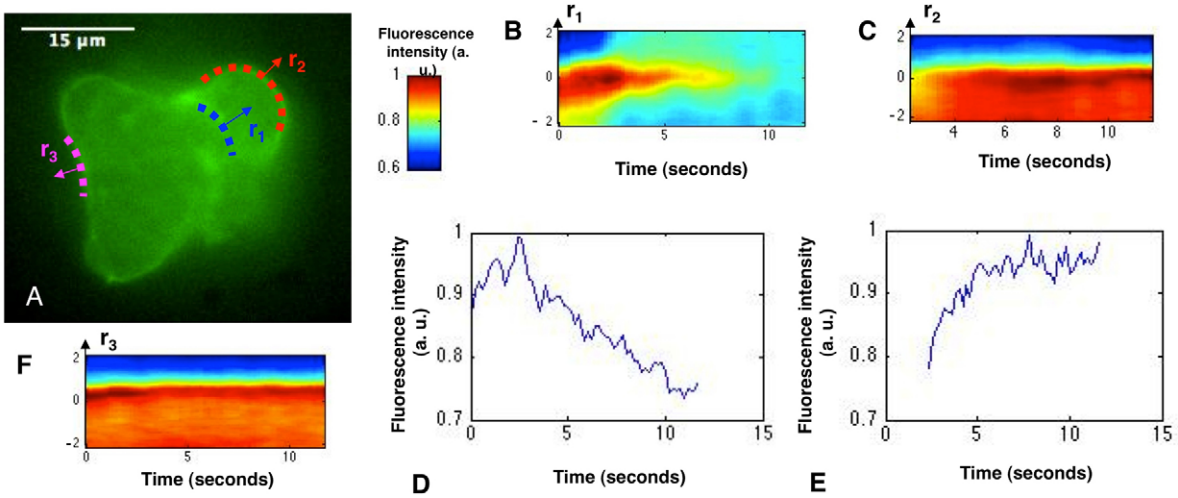

Fig. 4. Time course of actin polymerization/depolymerization during bleb formation. (**A**) The fluorescence signal (LifeAct–GFP) was analyzed in individual images over the initial cortex region (blue dashed line), at the bleb boundary (red dashed line) and at a remote position where the cortex is stationary (purple dashed line) (see Materials and Methods); r (r_1, r_2, r_3) represents the radial coordinate that can be locally defined perpendicular to the bleb contour. (**B**,**C**) The time course of fluorescence intensity along these lines is shown in kymographs. (**D**,**E**) Integration of the signal over the arc length is shown as a function of time. Over the 5–10 seconds following membrane disjunction, F-actin decays at the position of the initial cortex (B and D) but increases at the new front (C and E). (**F**) No other changes are seen.

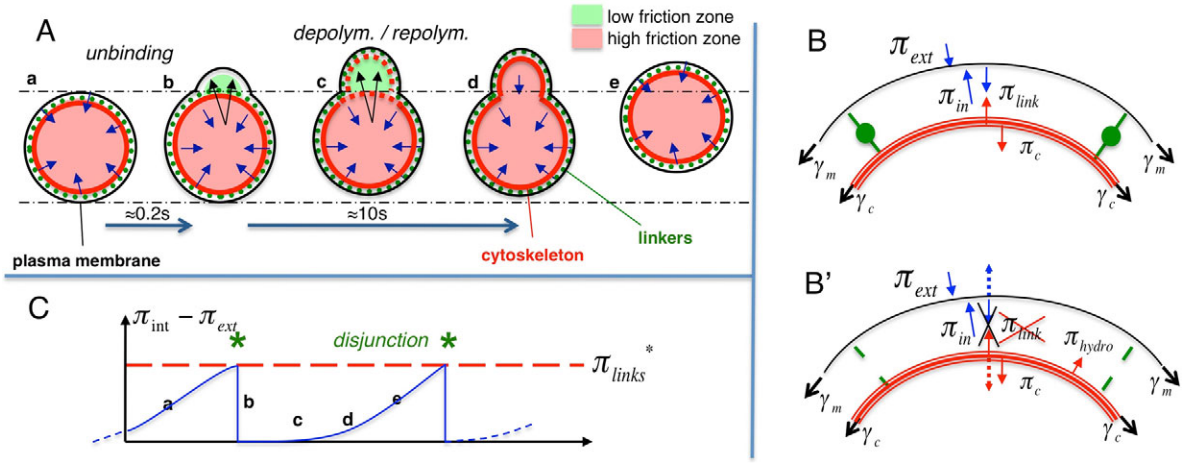

Fig. 5. Bleb-based motility. (**A**) Qualitative model of bleb-based motility. Blue arrows indicate direction of contraction and black arrows the direction of expansion. (a) Initial state, (b) plasma membrane detaches from the cytoskeleton, (c) depolymerization and repolymerization of actin, (d) new cortex has fully matured, (e) new position of cell. (**B**) The distribution of forces exerted on the cytoskeleton, the plasma membrane and molecular linkers. These forces are mainly: the hydrostatic outside π_{ext} and inside π_{in} pressures, the membrane tension γ_m, the cortical tension γ_c resulting in pressure π_c, and the forces exerted on and transmitted by individual linkers, resulting in pressure π_{link}. Arrows indicate the direction in which the forces act. (**B′**) Forces exerted during membrane disjunction. The linker pressure (π_{links}) on the membrane and its opposing cytoskeletal counterpart disappear. Dashed blue arrow indicates effective outward pressure and dashed red arrow the effective inward pressure. π_{hydro} is the outward pressure on the cortex. (**C**) The cyclic change in the inside–outside pressure difference over time. Letters a–e correspond to the states shown in A.

from the cytoskeleton, it is suddenly pushed forward by π^*_{links} and the cortex accordingly recoils inward under the effect of $-\pi^*_{links}$. Concomitantly, the excess internal pressure π_{int} relaxes locally. Next, the local pressure drop of π_{int} propagates throughout the cell and leads to small amplitude cytosolic motions. As the bleb stabilizes through actin polymerization and contraction, the pressure rises again until the next disjunction transition. Hence, the resulting cycle is essentially characterized by instability of the intracellular pressure. According to our model, the time between bleb formation events is determined by the rate of stress accumulation through contraction and by the tensile strength and density of the linkers. The resulting instability will be periodic if these biological control parameters remain constant. We have investigated two key predictions of this model: the respective roles of contractility and pressure, and the periodicity.

Respective roles of pressure effects and contraction

We first determined to what extent bleb formation was sensitive to external perturbations of the inside–outside pressure difference. Using micropipette aspiration (supplementary material Movie 9), we observed that the membrane region exposed to low external pressure (~–500 Pa) exhibited active blebbing, whereas the opposite end of the cell stopped making blebs. This strongly suggests that the inside–outside pressure difference is a key parameter in triggering membrane disjunction. In agreement with several previous reports (Arhets et al., 1998; Paluch et al., 2005; Charras et al., 2005), the inhibition of actomyosin contraction with ML-7 and Y27632 was found to block bleb formation (supplementary material Fig. S4B,D). To elucidate the respective roles of contraction and the pressure increase (both of which appear to be required for blebbing), we designed an experiment in which the inside–outside pressure difference was cancelled while the contractile machinery remained intact.

Electroporation is known to transiently permeate the cell membrane and can therefore be used in conjunction with a micropipette to cancel the hydrostatic pressure difference at will on the subcellular scale and with good temporal resolution. *Eh* cells were held in tight contact with the micropipette tip. The electrical resistance was in the order of 25–30 MΩ. In this situation, the cells produced blebs that immediately disappeared at the onset of electrical pulse trains (see supplementary material Movie 10). As long as pulses were maintained, the cells shrank (Fig. 6 and supplementary material Fig. S5). As soon as the pulses ceased, blebbing resumed within a few seconds. In addition, electroporation-induced shrinkage was absent when either of two actomyosin inhibitors (ML-7 and Y27632) were added to the medium (see supplementary material Movie 11). Taken together, these results indicate that the contraction machinery is not affected by electroporation but cannot alone induce blebs when the hydrostatic pressure difference is cancelled. Meanwhile, the fact that a normally membrane-impermeant dye (propidium iodide) penetrated into the cell suggests that pores are formed. Interestingly, dye influx systematically occurred through a single permeation point (see supplementary material Movie 12) located outside of the micropipette. Indeed, the effect of electroporation, as revealed by propidium iodide experiments (see supplementary material Movie 12), is to create pores at a single point, through which endoplasmic material immediately leaks out and through which the dye enters a few seconds later, before it equilibrates throughout the cell (supplementary material Fig. 12). The effect of pores is to cancel, at least locally, the contraction-induced pressure difference. The fact that the electroporation-induced local pressure relaxation is immediately followed by a global effect on bleb inhibition strongly suggests that membrane disruption and blebbing result from a direct pressure on the membrane and from linker rupture, and also that the local pressure drop immediately propagates throughout the cell.

Blebbing can be forced into a periodic mode

Assuming that the rate of contraction and linker strength and density are constant and uniform, our model predicts that blebs

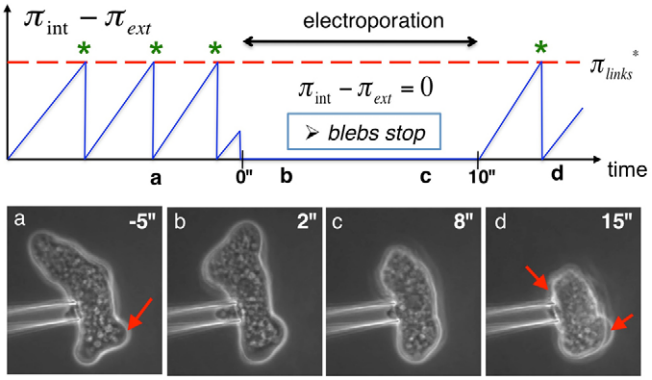

Fig. 6. Electroporation stops blebbing but not contraction. *Eh* cells (n=5) were held by a micropipette that delivers trains of electrical pulses (see Materials and Methods). Upper panel shows the change in the inside–outside pressure difference over time. Letters a–d indicate the time-points at which the images below were taken. (a) When no pulse is applied (t<0 seconds), the cell blebs as it does under normal conditions (Fig. 2 and supplementary material Movie 2). (b,c) As soon as electrical pulses are applied (0<t<10 seconds), blebbing stops and the cell shrinks. (d) Blebbing resumes as soon as electrical pulses cease. Arrows point to blebs.

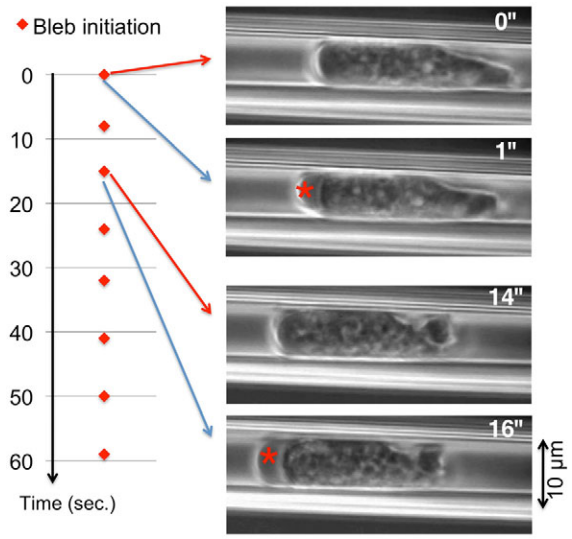

Fig. 7. Blebs become periodic in a static geometry. Using a low suction pressure (500 Pa), *Eh* cells were induced to move inside a 10-µm diameter micropipette. Saltatory motions were observed in time-lapse, phase-contrast videos (see supplementary material Movies 1–13). Successive membrane disjunctions (red asterisks) are clearly resolved in time. These transitions are illustrated by two pairs of images (0/1 seconds and 14/16 seconds). The time course of these transitions (red dots on the time axis) exhibits a clear periodicity of 8±2 seconds (n=46).

will be produced periodically. In cell-on-glass, blebs occurred one by one. There was neither time overlap (supplementary material Fig. S6) nor a well-defined period. Indeed, the blebs were heterogeneous in terms of duration and size (supplementary material Fig. S7) and the fluctuations over time were so large that no statistically meaningful period could be distinguished. According to our model, this temporal irregularity suggests that the control parameters are not constant over time and/or are not uniform in space. The simplest explanation is that the local pressure on the linkers (π_c) depends on the local membrane curvature, i.e. $\pi_c=2\gamma_c/R$ (Fig. 5B). Curvature is indeed strongly non-uniform in *Eh* cells (Fig. 2). Interestingly, when the cell is forced to adopt a more regular shape in micropipette aspiration experiments, a clear periodicity appears (Fig. 7). The period (8±2 seconds, n=46 blebs) matches that of the polymerization/depolymerization measured above. This clearly shows that blebbing frequency fluctuations are dominated by geometric effects and that the control parameters are constant. Our micropipette experiments have been extensively described in a detailed theoretical analysis of various dynamic modes for cortical instability (Brugues et al., 2010).

Discussion

Bleb formation is observed in apoptotic cells (Mills et al., 1998; Sebbagh et al., 2005; Leverrier and Ridley, 2001; Sebbagh et al., 2001), migrating cells (Blaser et al., 2006; Yoshida and Soldati, 2006), non-migrating cells (Keller and Eggli, 1998; Gutjahr et al., 2005; Charras et al., 2005; Paluch et al., 2005) and in cells before they fully adhere to a flat substrate (Norman et al., 2010). Nevertheless, the only previously reported situation in which motility is entirely driven by blebs is primordial germ cell (PGC) migration in zebrafish (Blaser et al., 2006; Raz and Reichman-Fried, 2006). The key message of the present work is that *Eh* cell migration (as with PGCs) is solely driven by blebbing, at least under the circumstances investigated here. However, unlike zebrafish PGCs (which are immobile in vitro), *Eh* cells exhibit bleb-based motility both in vitro and in vivo and therefore appear to constitute a unique model for investigating the mechanism of bleb formation and its relationship with motility in a relatively normal physiological context. We took advantage of this unique feature and used RICM to qualitatively elucidate the relationship between bleb formation and retraction, cell–substrate contact dynamics and net cell motion.

The present data and our previous observations on in vivo infection-related *Eh* cell motility (Coudrier et al., 2005) together strongly suggest that blebbing-based cell motion is efficient compared the well-known mesenchymal migration mode. We observed extremely high bleb front velocities: up to two orders of magnitude higher than the average speed for mesenchymal cells (Bray, 2001). Nevertheless, these velocities are transient and do not directly reflect average motility speed. Given that the *Eh* cell blebs are produce isotropically and lead to random motion (supplementary material Movie 13), the efficiency of motility is better reflected by the mean square displacement (supplementary material Fig. S8), which is typically in the order of 0.1–10 µm^2/second. One of the most remarkable features of *Eh* bleb-based motility is the very high blebbing frequency, which makes it possible for the cell to change direction several times per minute.

Comments on the blebbing model

In the initial state in the cycle (Fig. 5Aa), the cell is in a static situation in which the increasing stress does not translate into significant deformation. The internal pressure is uniform and one would expect to have a uniform distribution of the disjunction probability if the linker distribution and curvature are uniform. However, it should be borne in mind that linkers at the membrane cytoskeleton interface can be very dynamic (Coscoy et al., 2002); hence, density fluctuations can trigger local changes in the disruption pressure π_{link}. In a few reports, collapse of the cortex is seen as the first event. However, this situation has only been seen

in non-physiological situations (Keller and Eggli, 1998; Paluch et al., 2005).

In our present model, we decided to neglect the possible role of osmotic forces in membrane disruption and swelling. Osmotic forces have indeed been proposed to account for membrane swelling (Oster and Perelson, 1987) due to an outside–inside water flux. In the present situation, no such inward flux is seen. Instead, the swelling is accompanied throughout the whole cell by a small but detectable flow that is directed towards and then fills the bleb (supplementary material Fig. S9). Incidentally, this observation provides a strong indication that the local hydrostatic pressure drop induced at the time of membrane disjunction propagates immediately through the whole cell. This propagation uniformly relieves the pressure on the links and inhibits the formation of new blebs elsewhere. This hypothesis is in agreement with our observation (supplementary material Fig. S6) that (in general) new blebs only appear once the previous one has 'matured' back to the starting point. This mutual bleb exclusion [which has also been seen in zebrafish PGCs (Blaser et al., 2006)] might account for the relatively high observed diffusion coefficient.

Our data strongly suggest that contractility exerts overall control over the internal hydrostatic pressure and that this pressure remains uniform. As a consequence, a local increase in contractile activity alone is not likely to generate a sustained local pressure increase and thus trigger local bleb formation. This contradicts the interpretation of experiments in which bleb formation could be suppressed (Charras et al., 2005) by the local inhibition of contractility. These observations prompted Charras and coworkers to hypothesize that the cytoskeleton can display poroelastic behavior in which the hydraulic resistance and elasticity of the cytoskeleton results in relatively long propagation times for local pressure variations (10 seconds across the cell). This is obviously not the case with *Eh* cells, because local relaxation of the inside–outside pressure difference immediately cancelled blebbing throughout the cell, which suggests that a local hydrostatic pressure jump was relieved almost instantaneously. Furthermore, we observed that the cortex clearly moves inward upon blebbing (supplementary material Fig. S10). This recoil can be accounted for by the interplay of two antagonist pressures occurring during the disjunction: the loss of the pressure π_{links} exerted on the cytoskeleton, and the outward-directed pressure π_{hydro} due to the hydrodynamic resistance caused by the outward flow. Hence, the recoil of the cortex indicates that the linker pressure exceeds the viscous resistance and that poroelastic effects at the cytoskeleton–membrane junction can therefore be neglected. In addition, the observation that blebbing is immediately followed by a small but detectable granular flow throughout the whole cell (supplementary material Fig. S9) is also a strong indication that the local hydrostatic pressure drop induced by blebbing propagates almost instantaneously through the whole cell.

Our finding that myosin activity drives bleb formation in a non-local way via the overall internal hydrostatic pressure should also be considered in light of a report showing that blebs in zebrafish PGCs colocalize with hot spots of a calcium ionophore protein and thus coincide with local calcium increases and the accompanying contraction (Blaser et al., 2006). In these experiments, contraction was necessary to produce blebs but did not necessarily dictate their location. These blebs might result from a local reduction in linker density triggered by either calcium pulses or contraction-induced cortex heterogeneities. These previous observations are consistent with our hypothesis of a uniform hydrostatic pressure, but more detailed experiments are needed to distinguish between the possible mechanisms controlling bleb location.

Biochemical control of the dynamic instability

Our model is founded on three key parameters: (1) the rate at which pressure (due to actomyosin contraction and curvature) builds up, (2) the critical disjunction pressure (resisted by membrane–cytoskeleton linkers) and (3) the turnover rate of the actin cortex. The rate of pressure build-up depends on both the level of mechano-enzymatic activity and the cortex density. Therefore, in the presence of a structurally stable cortex, the time needed to reach the disjunction pressure is expected to vary inversely with the reciprocal of the contraction rate. However, the actin cortex is far from being a static structure (Pantaloni et al., 2001; Pollard and Borisy, 2003) and its turnover will certainly interfere with the pressure build-up. Indeed, each time a microfilament is lost through turnover, the accumulated stress disappears and is subtracted from the network stress. One therefore expects the tensile stress to reach a steady-state level that is modulated by the contraction rate and the actin turnover rate. This steady state will not be reached if disjunction occurs faster than stress saturation. In this context, the kinetic competition between contraction and polymerization rates (along with the critical disjunction pressure) should lead to different dynamic modes, with or without disjunction (supplementary material Fig. S11). Although a quantitative, theoretical investigation of these dynamic modes has been carried out (Brugues et al., 2010), the qualitative model developed here should help us to understand how blebbing is biochemically controlled.

Efficiency of motility and external mechanical control

Our RICM experiments showed that *Eh* cells even adhere to a bare glass slide, probably due to the relatively nonspecific nature of the molecular adhesive machinery of the parasite. If blebs are to produce motion in a viscoelastic environment, the sum of the net momentum successively transmitted to the substrate (first during bleb emission and then during the maturation/contraction steps) must be non-zero. During bleb emission, the opposing forces exerted on the bleb arise from either viscous drag in the liquid phase or from friction between the membrane and the substrate. Both types of forces are effectively counteracted by adhesion of the rest of the cell to the substrate, as suggested by the fact that the centre of mass does move forward during that phase. As the bleb matures, cortex polymerization and the formation of links with adhesion receptors result in a rather uniform solid-like friction. Upon further contraction, the centre of mass is therefore not expected to move. Qualitatively, the liquid-like structure of the bleb breaks the symmetry of the friction forces in space and time and thus powers net motion.

In addition to chemical signals, external mechanical factors could also direct bleb-based motion by restricting bleb emission in directions where blebs are not limited by contact pressure, such as the holes in the extracellular microenvironment. In principle, any factor that interferes with contraction-induced strain (such as adhesion to a rigid substrate) could limit the internal pressure build-up and thus inhibit bleb-based motility.

We hereby propose that the use of bleb-driven motility depends on the balance between contractile activity and the elastic compliance of the microenvironment (providing cell adhesion is strong enough to couple these forces). In addition to intracellular controls on motility (Lammermann and Sixt, 2009), we suggest that cells can be prompted to switch between bleb-driven and mesenchymal motility modes by changes in the surrounding milieu (namely the adhesiveness, geometry and elastic compliance). This

is an attractive concept that should help us to understand how cells optimize migration strategies in various 'soft' and 'stiff' microenvironments and enhance our knowledge of cellular behavior during embryogenesis, parasite infection, tumorigenesis and immune cell migration (Hugues et al., 2004; Coudrier et al., 2005; Raz and Reichman-Fried, 2006; Beadle et al., 2008).

Materials and Methods

Preparation of *Entamoeba histolytica* cells and drug treatments

E. histolytica HM1-IMSS (Diamond, 1961) wild-type strain was grown and resuspended in TY-SS3 medium before the experiments. For experiments in non-adhering conditions, cells were kept in suspension at the interface between a low density medium (culture medium) and a high density medium (Percoll, Sigma) corrected with calcium chloride to obtain the usual osmolarity of cell cultures (300 mOsm). Propidium iodide (Sigma) used for checking the membrane integrity during electroporation experiments was diluted to 2 μg/ml. Myosin activity was inhibited with ML-7 (Sigma) at 50 μM, and Y-27632 (Sigma) at 40 μM. Actin was stabilized (inhibition of depolymerization) by jasplakinolide (Interchim) at 200 nM. To keep anaerobic conditions, nitrogen was injected for at least 30 minutes in drug solutions before use. Because different cells can exhibit quite different behaviors, experiments with drugs were carried out in a comparative way, i.e. using the same cell prior to and after application of the drug. Therefore, individual cells must be kept in the observation field despite the fluid flow caused by the injection of drugs in the observation chamber. To this end, cells were protected from the flow by a thin metal grid (100 μm mesh size, Saulas) maintained 400 μm above the floor of the observation chamber by glass beads (Polysciences).

Scaling argument for the pressure velocity relationship

The scaling argument used to relate the expansion velocity to the pressure that drives it reads as follows: The Stokes equation between pressure gradient (through the cortex) and the viscous stress is $\delta P=\eta\xi v$, where δP is the pressure difference, v the fluid velocity, η the cytosol viscosity and ξ the mesh size. The pressure gradient is coupled to the pressure difference through the cortex by $\delta P/h=\delta P$, where h is the thickness of the cortex. Velocity gradients within the cortex are dictated by the cortex mesh size $\eta v=v\xi^{-2}$. Thus, the relationship between pressure difference and speed is $\delta P=\eta v h\xi^{-2}$. With $\eta=10^{-3}$ Pa seconds, v=10 μm/second, ξ=30–100 nm and h=1 μm, the value found for the pressure that drives the bleb is 1–10 Pa.

Live actin imaging of cytoskeleton

The actin cytoskeleton was seen by fluorescence video microscopy using the LifeAct peptide (MGVADLIKKFESISKEE) (Riedl et al., 2008) fused to GFP through a heptapeptide (GDPPVAT). This was achieved by PCR amplification using two oligonucleotides constructed to hybridize with each other through the complementary regions (underlined nucleotides) 5′-AT**GGTACC**ATGGGAGTTGCTGATCTTA-TTAAAAAATTCGAATCAATTTCAAAAGAAGAAG-3′ and 5′-AT**GGTACC**-AGTAGCAACTGGTGGATCTCCTTCTTCTTTTGAAATTGATTCG-3′. When hybridized, and amplified, the double-strand fragment contains the actin-binding peptide and the linker region, flanked by two *Kpn*I sites (bold nucleotides) for direct cloning into the pNeo-GFP vector.

Live imaging

Most observations were made with an inverted IX-70 Olympus microscope using LaCon POCmini observation chamber in 'open' configuration. The chamber was completely filled with medium and closed, to maintain anaerobic conditions over hours. Phase-contrast observation movies were recorded with a firewire AVT Guppy F-080B CCD camera with the BTV Pro acquisition software at a 15 Hz frame rate. Protrusions expand in 3D, but we choose to use 2D wide-field imaging to sustain a high acquisition rate. Because we used low magnification imaging, the depth of field was large enough to capture all protrusion. Fluorescence imaging was performed with a CoolSNAP HQ2 (Roper Scientific) CCD camera with Micro-Manager software. Fluorescence and phase contrast (or RICM/phase contrast) were acquired quasi-synchronously by sequential illumination (LEDs for bright field alternated with HBO Mercury lamp), using a home-made LabView program.

Micropipette experiments

Sample chambers were assembled as two clean glass coverslips glued with vacuum grease and fixed with nail polish to a 1-mm thick aluminum support. Once filled with cells and medium, the chamber was sealed with mineral oil to prevent water evaporation and limit oxygen entry. The chamber was placed on the stage of an inverted microscope (Axiovert 200, Zeiss), equipped with 60× Olympus UPlanFl immersion oil objective (1.25 NA) and a 0.8 NA air condenser. Temperature was regulated by a home-made water circulation around the objective, and fluid temperature was regulated by a thermostated circulator. A homemade micromanipulator was clamped on the microscope, and micropipettes of about 10 μm tip diameter were connected to a mobile water tank. Phase-contrast images were collected by an analog CCD camera (XC-ST70CE, Sony). Micropipette-based electroporation was performed with the 800A Axoporator. Pulse trains of alternating polarity were used to avoid a permanent current bias and hydrolysis. Electroporation conditions are defined by the pulse amplitude (V_0), the pulse duration (τ), the pulse repetition frequency (f) and the train duration (T). Typical values of these parameters are: V_0 ±6 V, τ 1 ms, f 100 Hz, and T 10 seconds. The typical resistance of micropipette was 20 MΩ.

Image analysis

Several Matlab routines were specifically developed for image analysis. Because the structure of the contrast at the cell boundary varies with time, especially for phase contrast imaging, the use of constant parameters (threshold, gradient, etc.) was not accurate enough. We developed instead an autocorrelation algorithm that is embedded in the program that directly processes movies. Fluorescence images of Fig. 4 could not be processed by the autocorrelation method, and edges were manually determined frame by frame. Kymographs were constructed as follows: for each time point, we represented the average radial distribution of the fluorescence intensity obtained by averaging over the contour.

The authors would like to acknowledge Elisabeth Labruyere and Christophe Zimmer (Institut Pasteur, Paris) for fruitful discussions on the biology of *Eh* and image analysis, Christian Weber for preparing the LifeAct construct, Sylvie Syan for the parasite culture, Isabel Llano and Jeremie Barral for their help during electroporation experiments, Vincent Semetey together with Pia Streicher for helping with surface treatments, and Gil Toombes for critical reading of the manuscript. B.M. and F.A. are members of GdR CellTiss of the CNRS. B.M. was supported by a doctoral fellowship from Region Ile-de-France. This work was supported by grants from the ANR (to N.G. and F.A., to P.N. and P.S.), the Institut Curie and the Region Ile-de-France.

Supplementary material available online at
http://jcs.biologists.org/cgi/content/full/123/XX/XXXX/DC1

References

Arhets, P., Olivo, J. C., Gounon, P., Sansonetti, P. and Guillen, N. (1998). Virulence and functions of myosin II are inhibited by overexpression of light meromyosin in *Entamoeba histolytica*. *Mol. Biol. Cell* **9**, 1537-1547.

Beadle, C., Assanah, M. C., Monzo, P., Vallee, R., Rosenfeld, S. S. and Canoll, P. (2008). The role of myosin ii in glioma invasion of the brain. *Mol. Biol. Cell* **19**, 3357-3368.

Bell, G. I. (1978). Models for the specific adhesion of cells to cells. *Science* **200**, 618-627.

Blaser, H., Reichman-Fried, M., Castanon, I., Dumstrei, K., Marlow, F. L., Kawakami, K., Solnica-Krezel, L., Heisenberg, C. P. and Raz, E. (2006). Migration of zebrafish primordial germ cells: a role for myosin contraction and cytoplasmic flow. *Dev. Cell* **11**, 613-627.

Blazquez, S., Zimmer, C., Guigon, G., Olivo-Marin, J. C., Guillen, N. and Labruyere, E. (2006). Human tumor necrosis factor is a chemoattractant for the parasite *Entamoeba histolytica*. *Infect. Immunol*. **74**, 1407-1411.

Bray, D. (2001). *Cell Movement,* 2nd edn. London: Garland.

Brugues, J., Maugis, B., Casademunt, J., Nassoy, P., Amblard, F. and Sens, P. (2010). Dynamical organization of the cytoskeletal cortex probed by micropipette aspiration. *Proc Natl Acad Sci USA* **107**, 15415-15420.

Carragher, N. O., Walker, S. M., Scott Carragher, L. A., Harris, F., Sawyer, T. K., Brunton, V. G., Ozanne, B. W. and Frame, M. C. (2006). Calpain 2 and Src dependence distinguishes mesenchymal and amoeboid modes of tumour cell invasion: a link to integrin function. *Oncogene* **25**, 5726-5740.

Charras, G. and Paluch, E. (2008). Blebs lead the way: how to migrate without lamellipodia. *Nat. Rev. Mol. Cell Biol*. **9**, 730-736.

Charras, G. T., Yarrow, J. C., Horton, M. A., Mahadevan, L. and Mitchison, T. J. (2005). Non-equilibration of hydrostatic pressure in blebbing cells. *Nature* **435**, 365-369.

Coscoy, S., Waharte, F., Gautreau, A., Martin, M., Louvard, D., Mangeat, P., Arpin, M. and Amblard, F. (2002). Molecular analysis of microscopic ezrin dynamics by two-photon frap. *Proc. Natl. Acad. Sci. USA* **99**, 12813-12818.

Coudrier, E., Amblard, F., Zimmer, C., Roux, P., Olivo-Marin, J. C., Rigothier, M. C. and Guillen, N. (2005). Myosin II and the Gal-GalNAc lectin play a crucial role in tissue invasion by *Entamoeba histolytica*. *Cell. Microbiol*. **7**, 19-27.

Diamond, L. S. (1961). Axenic cultivation of entamoeba hitolytica. *Science* **134**, 336-337.

Fackler, O. T. and Grosse, R. (2008). Cell motility through plasma membrane blebbing. *J. Cell Biol.* **181**, 879-884.

Friedl, P. (2004). Prespecification and plasticity: shifting mechanisms of cell migration. *Curr. Opin. Cell Biol.* **16**, 14-23.

Friedl, P. and Wolf, K. (2003). Tumour-cell invasion and migration: diversity and escape mechanisms. *Nat. Rev. Cancer* **3**, 362-374.

Friedl, P., Borgmann, S. and Brocker, E. B. (2001). Amoeboid leukocyte crawling through extracellular matrix: lessons from the dictyostelium paradigm of cell movement. *J. Leukoc. Biol*. **70**, 491-509.

Gonzalez-Robles, A. and Martinez-Palomo, A. (1983). Scanning electron microscopy of attached trophozoites of pathogenic entamoeba histolytica. *J. Protozool*. **30**, 692-700.

Gutjahr, M. C., Rossy, J. and Niggli, V. (2005). Role of Rho, Rac, and Rho-kinase in phosphorylation of myosin light chain, development of polarity, and spontaneous migration of Walker 256 carcinosarcoma cells. *Exp. Cell Res.* **308**, 422-438.

Hugues, S., Fetler, L., Bonifaz, L., Helft, J., Amblard, F. and Amigorena, S. (2004). Distinct T cell dynamics in lymph nodes during the induction of tolerance and immunity. *Nat. Immunol*. **5**, 1235-1242.

Keller, H. and Eggli, P. (1998). Protrusive activity, cytoplasmic compartmentalization, and restriction rings in locomoting blebbing Walker carcinosarcoma cells are related to detachment of cortical actin from the plasma membrane. *Cell Motil. Cytoskeleton* **41**, 181-193.

Keller, H., Rentsch, P. and Hagmann, J. (2002). Differences in cortical actin structure and dynamics document that different types of blebs are formed by distinct mechanisms. *Exp. Cell Res*. **277**, 161-172.

Lammermann, T. and Sixt, M. (2009). Mechanical modes of 'amoeboid' cell migration. *Curr. Opin. Cell Biol*. **21**, 636-644.

Leverrier, Y. and Ridley, A. J. (2001). Apoptosis: caspases orchestrate the rock 'n' bleb. *Nat. Cell Biol*. **3**, E91-E93.

Mierke, C. T., Rosel, D., Fabry, B. and Brabek, J. (2008). Contractile forces in tumor cell migration. *Eur. J. Cell Biol*. **87**, 669-676.

Mills, J. C., Stone, N. L., Erhardt, J. and Pittman, R. N. (1998). Apoptotic membrane blebbing is regulated by myosin light chain phosphorylation. *J. Cell Biol*. **140**, 627-636.

Mills, J. C., Stone, N. L. and Pittman, R. N. (1999). Extranuclear apoptosis. the role of the cytoplasm in the execution phase. *J. Cell Biol*. **146**, 703-708.

Norman, L. L. , Brugues, J. Sengupta, K., Sens, P. and Aranda-Espinoza, H. (2010). Cell blebbing and membrane area homeostasis in spreading and retracting cells. *Biophys. J.* **99**, 1726–1733.

Oster, G. F. and Perelson, A. S. (1987). The physics of cell motility. *J. Cell Sci.* **8**, 35-54.

Paluch, E., Piel, M., Prost, J., Bornens, M. and Sykes, C. (2005). Cortical actomyosin breakage triggers shape oscillations in cells and cell fragments. *Biophys. J.* **89**, 724-733.

Pantaloni, D., Le Clainche, C. and Carlier, M. F. (2001). Mechanism of actin-based motility. *Science* **292**, 1502-1506.

Pollard, T. D. (1986). Rate constants for the reactions of ATP- and ADP-actin with the ends of actin filaments. *J. Cell Biol*. **103**, 2747-2754.

Pollard, T. D. and Borisy, G. G. (2003). Cellular motility driven by assembly and disassembly of actin filaments. *Cell* **112**, 453-465.

Raz, E. and Reichman-Fried, M. (2006). Attraction rules: germ cell migration in zebrafish. *Curr. Opin. Genet. Dev.* **16**, 355-359.

Riedl, J., Crevenna, A. H., Kessenbrock, K., Yu, J. H., Neukirchen, D., Bista, M., Bradke, F., Jenne, D., Holak, T. A., Werb, Z. et al. (2008). Lifeact: a versatile marker to visualize F-actin. *Nat. Methods* **5**, 605-607.

Sahai, E. (2007). Illuminating the metastatic process. *Nat. Rev. Cancer* **7**, 737-749.

Sebbagh, M., Renvoize, C., Hamelin, J., Riche, N., Bertoglio, J. and Breard, J. (2001). Caspase-3-mediated cleavage of ROCK I induces MLC phosphorylation and apoptotic membrane blebbing. *Nat. Cell Biol*. **3**, 346-352.

Sebbagh, M., Hamelin, J., Bertoglio, J., Solary, E. and Breard, J. (2005). Direct cleavage of ROCK II by granzyme B induces target cell membrane blebbing in a caspase-independent manner. *J. Exp. Med*. **201**, 465-471.

Stanley, S. L. (2001). Pathophysiology of amoebiasis. *Trends Parasitol*. **17**, 280-285.

Stanley, S. L. (2003). Amoebiasis. *Lancet* **361**, 1025-1034.

Theriot, J. A., Mitchison, T. J., Tilney, L. G. and Portnoy, D. A. (1992). The rate of actin-based motility of intracellular listeria monocytogenes equals the rate of actin polymerization. *Nature* **357**, 257-260.

Tilney, L. G. and Inoue, S. (1985). Acrosomal reaction of the thyone sperm. iii. the relationship between actin assembly and water influx during the extension of the acrosomal process. *J. Cell Biol*. **100**, 1273-1283.

Yoshida, K. and Soldati, T. (2006). Dissection of amoeboid movement into two mechanically distinct modes. *J. Cell Sci.* **119**, 3833-3844.

Zaki, M., Andrew, N. and Insall, R. H. (2006). *Entamoeba histolytica* cell movement: a central role for self-generated chemokines and chemorepellents. *Proc. Natl. Acad. Sci. USA* **103**, 18751-18756.